

Rate Coefficients of C₂H with C₂H₄, C₂H₆, and H₂ from 150 to 359 K

Brian J. Opansky and Stephen R. Leone*[†]

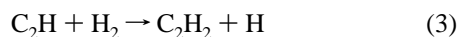
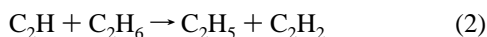
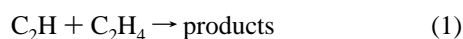
JILA, National Institute of Standards and Technology and University of Colorado,
Department of Chemistry and Biochemistry, University of Colorado, Boulder, Colorado 80309-0440

Received: July 2, 1996; In Final Form: October 3, 1996[⊗]

Rate coefficients for the reactions C₂H with C₂H₄, C₂H₆, and H₂ are measured over the temperature range 150–359 K using transient infrared laser absorption spectroscopy. The ethynyl radical is formed by photolysis of C₂H₂ with a pulsed excimer laser at 193 nm, and its transient absorption is monitored with a color center laser on the Q₁₁(9) line of the A²Π–X²Σ transition at 3593.68 cm⁻¹. Over the experimental temperature range 150–359 K the rate constants of C₂H with C₂H₄, C₂H₆, and H₂ can be fit to the Arrhenius expressions $k_{\text{C}_2\text{H}_4} = (7.8 \pm 0.6) \times 10^{-11} \exp[(134 \pm 44)/T]$, $k_{\text{C}_2\text{H}_6} = (3.5 \pm 0.3) \times 10^{-11} \exp[(2.9 \pm 16)/T]$, and $k_{\text{H}_2} = (1.2 \pm 0.3) \times 10^{-11} \exp[(-998 \pm 57)/T] \text{ cm}^3 \text{ molecule}^{-1} \text{ s}^{-1}$, respectively. The data for C₂H with C₂H₄ and C₂H₆ indicate a negligible activation energy to product formation shown by the mild negative temperature dependence of both reactions. When the H₂ data are plotted together with the most recent high-temperature results from 295 to 854 K, a slight curvature is observed. The H₂ data can be fit to the non-Arrhenius form $k_{\text{H}_2} = 9.2 \times 10^{-18} T^{2.17 \pm 0.50} \exp[(-478 \pm 165)/T] \text{ cm}^3 \text{ molecule}^{-1} \text{ s}^{-1}$. The curvature in the Arrhenius plot is discussed in terms of both quantum mechanical tunneling of the H atom from H₂ to the C₂H radical and bending mode contributions to the partition function.

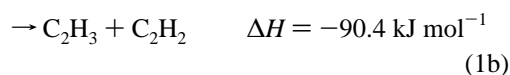
Introduction

The ethynyl radical, C₂H, is of fundamental importance in combustion chemistry and in planetary atmospheres.^{1–3} The ethynyl radical is a reactive intermediate in the pyrolysis of acetylene at temperatures in excess of 1800 K. It is also a reactive species on Titan, a moon of Saturn, where the atmospheric temperature is altitude-dependent (94 K at the surface and 160 K at 300 km above the surface).² To understand the importance of various ethynyl reactions in the two drastically different environments, it is desirable to know the rate coefficients for C₂H with such species as C₂H₄, C₂H₆, and H₂ over an extremely broad temperature range. In this work we are able to provide the first experimental data on low-temperature rate coefficients of the reactions



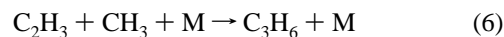
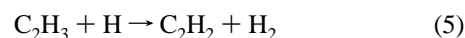
using transient infrared laser absorption spectroscopy.

The exothermicity of reaction 1 is such that there are two different thermodynamically accessible product channels available^{3–5}



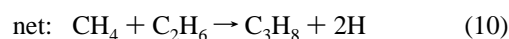
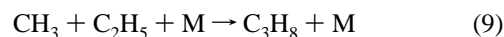
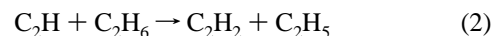
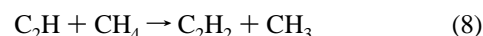
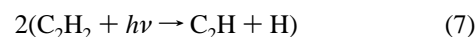
The C₄H₄ species in reaction 1a is the vinyl acetylene isomer. Reaction 1b is a possible source of vinyl radicals, C₂H₃, in Titan's atmosphere. It has been proposed by Yung *et al.*² that

vinyl radicals can undergo a disproportionation reaction to form acetylene and ethylene, scavenge a hydrogen atom, or act as a source of C₃ compounds:



The vinyl radical, like the ethynyl radical, is one of many species responsible for the synthesis of higher hydrocarbons in Titan's atmosphere through reactions with other molecules (C₂H₂, CH₄, C₂H₆, and C₂H₄ just to name a few). Reactions 4 and 6 are just a few examples of the hundreds of possible combinations of radical–radical reactions for which low-temperature rate coefficients are not known.

The reaction of C₂H + C₂H₆ leads to the production of ethyl radicals, C₂H₅, which opens pathways for the production of propane, C₃H₈, in Titan's atmosphere via the following scheme:^{2,6}



In addition, a pressure-dependent study by Lander *et al.*⁷ indicated a slight increase in $k_{\text{C}_2\text{H}_6}(\text{C}_2\text{H} + \text{C}_2\text{H}_6)$ with increasing helium number density. If this finding is valid, it raises new questions as to the mechanism involved, which may include the formation of an addition complex.

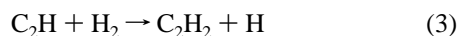
Since the room temperature rate constant for C₂H + H₂ is very slow and difficult to measure accurately, scientists interested in modeling planetary atmospheres have had to rely

* To whom correspondence should be addressed.

[†] Staff Member, Quantum Physics Division, National Institute of Standards and Technology.

[⊗] Abstract published in *Advance ACS Abstracts*, November 15, 1996.

on theoretical calculations or extrapolations from high-temperature data. For example, the reaction of



is listed in the proposed scheme of Yung *et al.* as contributing to the production of C₂H₆ in the atmospheres of both Jupiter and Saturn.^{2,3,6}

The reaction of C₂H + H₂ has been studied theoretically by both Harding *et al.*⁸ and Herbst.⁹ Harding and co-workers calculated k_{H_2} with Wigner tunneling corrections, from 300 to 2000 K for reaction 3 as $6.8 \times 10^{-19} T^{2.39} \exp[-435/T] \text{ cm}^3 \text{ molecule}^{-1} \text{ s}^{-1}$. The calculated fit shows significant curvature in the Arrhenius plot. Herbst calculated low-temperature rate coefficients for reaction 3 from 10 to 300 K using statistical phase space theory. The rate coefficients, k_{H_2} , are calculated with and without tunneling contributions. There is a steady decrease in k_{H_2} from 300 to 40 K, but the calculation with tunneling contributions shows that k_{H_2} begins to increase from $\sim 1.2 \times 10^{-15} \text{ cm}^3 \text{ molecule}^{-1} \text{ s}^{-1}$ at 40 K to $2.2 \times 10^{-15} \text{ cm}^3 \text{ molecule}^{-1} \text{ s}^{-1}$ at 10 K. For the nontunneling contribution calculation, k_{H_2} decreases rapidly from $1 \times 10^{-13} \text{ cm}^3 \text{ molecule}^{-1} \text{ s}^{-1}$ at 300 K to $\sim 6 \times 10^{-16} \text{ cm}^3 \text{ molecule}^{-1} \text{ s}^{-1}$ at 150 K. Clearly, more theoretical and experimental work is needed to determine whether or not tunneling plays a large enough role to "see" its effect on k_{H_2} with temperature. The goal in studying C₂H + H₂ reaches beyond measuring accurate rate coefficients for photochemical models. The objective is to distinguish any experimental evidence for tunneling at low temperatures and provide a basis for more theoretical work on this fundamental reaction.

Extrapolations of rate coefficients from high-temperature data can lead to significant errors at low temperatures due to a negative temperature dependence in certain reactions, as was shown for C₂H + C₂H₂.¹⁰ Several groups have measured rate coefficients for C₂H with C₂H₄, C₂H₆, and H₂ at 300 K or at higher temperatures.^{7,11–19} Up to this point, there have been no temperature-dependent rate coefficient measurements of C₂H with C₂H₄ and C₂H₆, and despite the importance of C₂H + H₂, there remains no experimental rate coefficient data for this reaction at low temperature.

The Arrhenius plot for reaction 1 shows a mild negative temperature dependence from 150 to 359 K. In addition, reaction 2 shows little or no temperature dependence of its rate coefficients over 153–357 K. Both sets of data are fit to Arrhenius expressions in which $k_{\text{C}_2\text{H}_4}$ and $k_{\text{C}_2\text{H}_6}$ are given by $(7.8 \pm 0.6) \times 10^{-11} \exp[(134 \pm 44)/T]$ and $(3.5 \pm 0.3) \times 10^{-11} \exp[(2.9 \pm 16)/T] \text{ cm}^3 \text{ molecule}^{-1} \text{ s}^{-1}$, respectively. The data for C₂H + H₂ show a positive temperature dependence from 178 to 359 K which can be fit to the Arrhenius expression $k_{\text{H}_2} = (1.2 \pm 0.3) \times 10^{-11} \exp[(-998 \pm 57)/T] \text{ cm}^3 \text{ molecule}^{-1} \text{ s}^{-1}$, but when combined with previous high-temperature measurements, there is evidence for curvature in the Arrhenius plot.

Experimental Section

The rate coefficients for C₂H with C₂H₄, C₂H₆, and H₂ are measured using transient infrared laser absorption spectroscopy. A schematic of the experimental setup is shown in Figure 1. The details of this setup have been described in numerous papers by this group so only a brief outline will be given here.^{10,20,21}

Ethynyl radicals are produced in the meter long, temperature variable flow cell at 193 nm by a pulsed excimer laser which was run at 55 mJ/pulse at 10 Hz. The absorption cell is constructed from quartz with Brewster windows for a multipass setup. The cell consists of an inner zone and an outer volume. In the inner jacket, the gases flow across the photolysis region

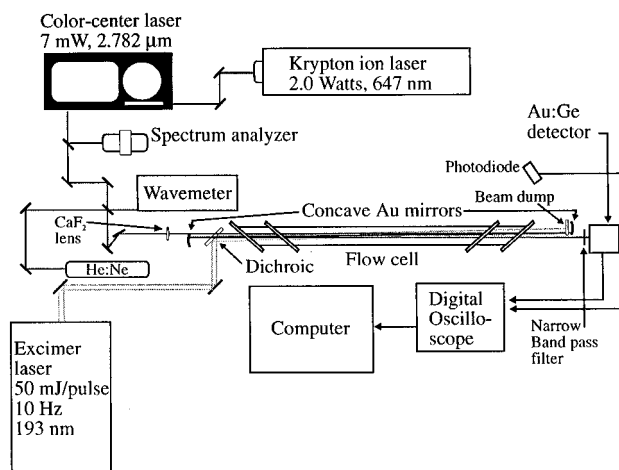


Figure 1. Schematic of experimental setup.

through a series of transverse inlets and outlets. The transverse flow arrangement allows high laser repetition rates with minimal photolysis of the same gas volume. With a typical flow rate of $2.7 \times 10^{20} \text{ molecules s}^{-1}$, the photolysis volume is replenished every 12 laser pulses. After accounting for UV laser loss on the Brewster windows of the cell, the C₂H concentration was estimated to be no greater than $7.5 \times 10^{10} \text{ cm}^{-3}$ for the highest acetylene pressures. (The acetylene number density ranges from 1.3×10^{14} to $4.8 \times 10^{14} \text{ cm}^{-3}$.) This estimation is based on using $1.35 \times 10^{-19} \text{ cm}^2$ for the absorption cross section at 193 nm²² and 0.26 for the quantum yield for C₂H production.²³ A 1500–6000-fold excess of C₂H₄, C₂H₆, or H₂ with respect to C₂H is always present in these experiments. Contributions from radical–radical or secondary reactions can be neglected since the time between collisions for C₂H and C₂H₄, C₂H₆, or H₂ is 1000 times shorter than the time between collisions of two C₂H radicals. Rate coefficients are measured at various ethene/ethane densities of $(0.2–5.2) \times 10^{15} \text{ cm}^{-3}$ and hydrogen densities of $(0.6–9.0) \times 10^{17} \text{ cm}^{-3}$. The helium density is varied over the range $(0.5–2.7) \times 10^{18} \text{ cm}^{-3}$ to test for a pressure dependence in the rate coefficients of C₂H with C₂H₄, C₂H₆, or H₂.

In the outer jacket either cooled pentane or isopentane is circulated by a micropump to achieve temperatures as low as 150 K. (It should be noted that not every rate coefficient can be measured down to 150 K because of the low C₂H₂ concentrations required to keep $k_{\text{C}_2\text{H}_2}[\text{C}_2\text{H}_2]$ contributions below 40%.) In experiments performed above room temperature, heated water was circulated around the inner cell.

The C₂H radical is probed in absorption by a high-resolution color center laser tuned to the Q₁₁(9) line at 3593.68 cm^{-1} of the A²Π–X²Σ transition.¹¹ A scanning Fabry-Perot spectrum analyzer is used to ensure the color center is running on one longitudinal mode, and a home-built scanning Michelson interferometer wavenumber is used to monitor the color center's wavelength.

The probe beam, after three to five multipasses, is directed onto a 50 MHz Ge:Au detector which has a 20 mm² sensitive area. Transient decay traces typically have a signal-to-noise ratio of 10–15 and are amplified and then coadded by a 100 MHz digital oscilloscope. Typical data collection consists of averaging the transient signal for 1500–2000 excimer pulses.

All gases used in this experiment flow through a mixing cell before entering the low-temperature cell. Helium is used to thermally equilibrate the gas mixture with the cell walls. All gases are obtained commercially with the following purities: He, 99.99%; C₂H₂, 99.6%; H₂, 99.9999%. The acetone is

removed from the acetylene by an activated charcoal filter. The temperature of the gas mixture is measured by a series of three type K thermocouples along the length of the cell. One thermocouple is inserted at each end of the cell, and the other is placed in the middle of the cell. This configuration is chosen to ensure that there are no thermal gradients along the length of the cell. Partial pressures of each gas are determined by calibrated mass flow meters and the measured total pressure inside the cell.

Analysis of Kinetic Data

The ethynyl radical is monitored directly from its ground state $C_2H(X^2\Sigma^+(0,0,0))$. In addition, it is necessary that the upper states of C_2H are fully quenched before the reaction of $C_2H(X^2\Sigma^+(0,0,0))$ with C_2H_4 , C_2H_6 , and H_2 occurs. Previous experiments by Lander *et al.*⁷ and Farhat *et al.*,¹¹ performed under similar conditions, have shown that relaxation of the $C_2H(X(0,0,1))$ state occurs in approximately $1 \mu s$. In this study, as well as in theirs, the reaction of $C_2H(X^2\Sigma^+(0,0,0))$ with C_2H_4 , C_2H_6 , and H_2 takes place over tens of microseconds. Therefore, complete vibrational relaxation should have occurred before any ground state measurements were made. To further ensure complete vibrational relaxation of C_2H , the fits only include data for $t > 3\tau_{rise}$.

The rate coefficients measured in this study are done under pseudo-first-order conditions in which $[X]$ (where $X = C_2H_4$, C_2H_6 , or H_2) and $[C_2H_2] \gg [C_2H]$. The rate of change of $[C_2H]$ can be expressed as

$$d[C_2H]/dt = -[C_2H](k_X[X] + k_{C_2H_2}[C_2H_2]) \quad (11)$$

After integration, this yields

$$[C_2H]_t = [C_2H]_0 \exp[-k_{obs}t] \quad (12)$$

where

$$k_{obs} = k_X[X] + k_{C_2H_2}[C_2H_2] \quad (13)$$

$$k_{obs} - k_{C_2H_2}[C_2H_2] = k_X[X] = k'_X \quad (14)$$

The observed decay rates, k_{obs} , are obtained by fitting the averaged transient signal to a single-exponential decay plus a constant, eq 15, to fit the arbitrary offset of the base line; see Figure 2.

$$y = A \exp(-k_{obs}t) + \text{constant} \quad (15)$$

The values of k_{obs} are corrected for the $C_2H + C_2H_2$ contribution taken from our own work¹⁰ by subtraction in eq 14. The resulting k'_X values are plotted against their respective X concentrations, and a linear least-squares fit is used to determine k_X ; see Figures 3 and 4. Errors in k_X are calculated by combining the accumulated uncertainties in the corrected decay fits, which includes errors in $k_{C_2H_2}$, with the uncertainties in temperature and in measuring the X concentration. The error in k_X is typically 15–25%.

Table 1 summarizes the measured rate coefficients for C_2H with C_2H_4 , C_2H_6 , and H_2 from 150 to 359 K. The data for C_2H with C_2H_4 and C_2H_6 are plotted in Figure 5 and indicate a slight negative temperature dependence for $k_{C_2H_4}$ and almost no temperature dependence for $k_{C_2H_6}$ over the temperature range 150–357 K. Both sets of data are fit to Arrhenius expressions in which $k_{C_2H_4}$ and $k_{C_2H_6}$ are given by $(7.8 \pm 0.6) \times 10^{-11} \exp[-(134 \pm 44)/T]$ and $(3.5 \pm 0.3) \times 10^{-11} \exp[(2.9 \pm 16)/T]$ $\text{cm}^3 \text{ molecule}^{-1} \text{ s}^{-1}$, respectively. The rate coefficients for $C_2H + H_2$ show a positive temperature dependence from 178 to 359 K

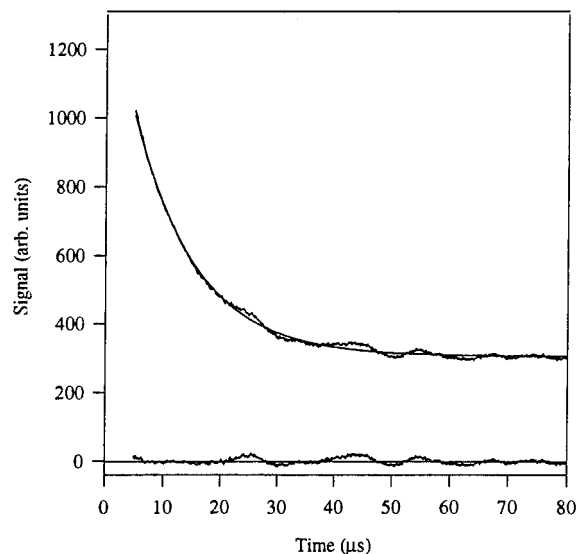


Figure 2. C_2H decay and fit due to reaction with C_2H_4 (upper curve). The lower plot is the residuals to the single-exponential decay.

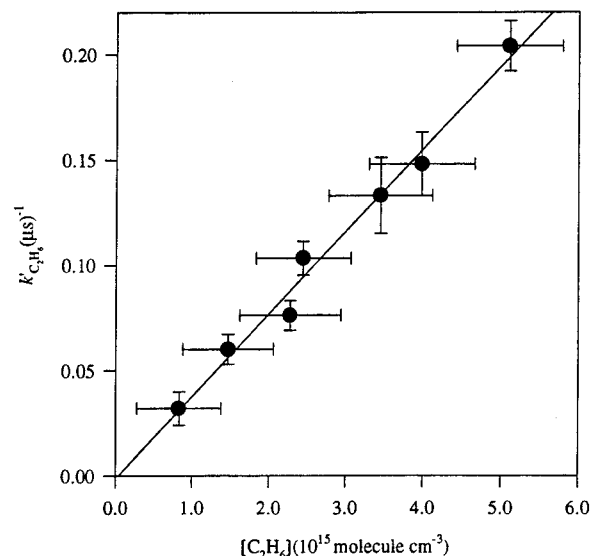


Figure 3. Plot of $k'_{C_2H_6}$ versus $[C_2H_6]$ at 198 K. The rate coefficient $k_{C_2H_6}$ is equal to $(3.9 \pm 0.6) \times 10^{-11} \text{ cm}^3 \text{ molecule}^{-1} \text{ s}^{-1}$.

which can be fit to the Arrhenius expression $k_{H_2} = (1.2 \pm 0.3) \times 10^{-11} \exp[(-998 \pm 57)/T]$ $\text{cm}^3 \text{ molecule}^{-1} \text{ s}^{-1}$; see Figure 6. In addition, no pressure dependence is found for the reactions of C_2H with C_2H_4 , C_2H_6 , or H_2 over the experimental conditions at 300 K.

Discussion

$C_2H + C_2H_4$ and C_2H_6 . In the case of $C_2H + C_2H_4$, the negative temperature dependence and lack of a pressure dependence is attributed to a short-lived addition complex which undergoes unimolecular dissociation to products before it can be stabilized. The rate coefficient measured at 150 K is lower than the one measured at 173 K, but the difficulty in measuring $k_{C_2H_4}$ at 150 K, due to the low C_2H_2 concentrations required, degrades the transient absorption signal. One cannot say with confidence that the measured rate coefficient at 150 K for $C_2H + C_2H_4$ is significant, for example, representing a small barrier to a C_4H_5 complex.

The rate coefficient $k_{C_2H_6}$ exhibits no temperature dependence from 153 to 357 K, comparable to that of $k_{CN+C_2H_6}$ from 75 to 300 K,²⁴ and no pressure dependence with varying helium densities. Since the current experimental setup prevents reach-

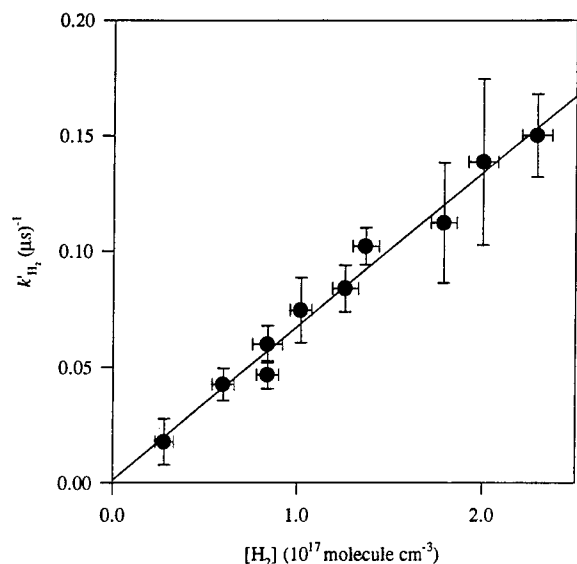


Figure 4. Plot of k'_{H_2} versus $[H_2]$ at 355 K. The slope of this plot is equal to $(6.7 \pm 0.9) \times 10^{-13} \text{ cm}^3 \text{ molecule}^{-1} \text{ s}^{-1}$.

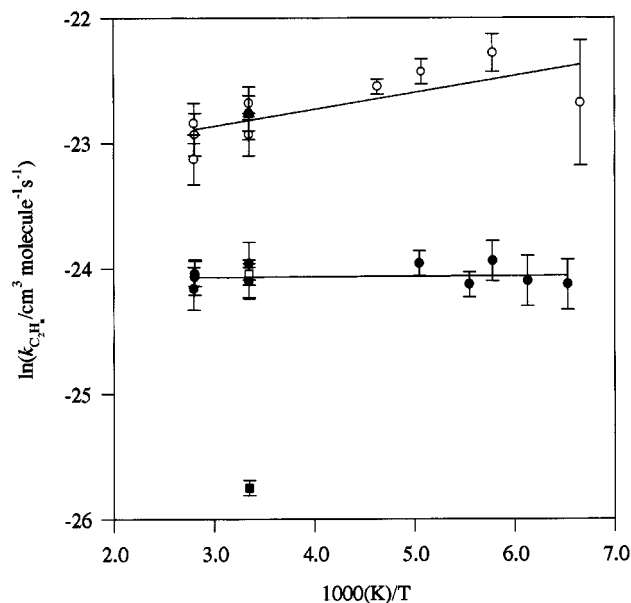


Figure 5. Arrhenius plot of C₂H with C₂H₄ and C₂H₆: ○, this work for C₂H + C₂H₄; ●, this work for C₂H + C₂H₆; ▲, Lander *et al.* for C₂H + C₂H₄; □, Lander *et al.* for C₂H + C₂H₆; ■, Laufer. The Arrhenius fit to C₂H with C₂H₄ and C₂H₆ is $(7.8 \pm 0.6) \times 10^{-11} \exp[-(134 \pm 44)/T]$ and $(3.5 \pm 0.3) \times 10^{-11} \exp[(2.9 \pm 16)/T] \text{ cm}^3 \text{ molecule}^{-1} \text{ s}^{-1}$, respectively.

ing temperatures lower than ~ 140 K, one cannot predict whether $k_{C_2H_6}$ will increase as does $k_{CN+C_2H_6}$. The lack of temperature and pressure dependences is attributed to an addition-elimination mechanism with little or no barrier to formation of the

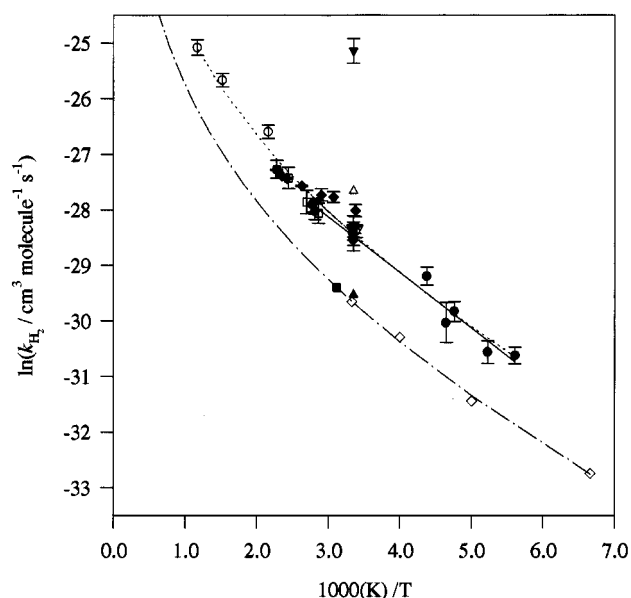


Figure 6. Arrhenius plot of C₂H + H₂: ●, this work; ○, Farhat *et al.*; □, Koshi *et al.*; ■, Lange *et al.*; ▲, Laufer *et al.*; ▼, Renlund *et al.*; △, Okabe; ◆, Peeters *et al.*; ▽, Herbst calculation. The solid line is the Arrhenius fit to this work and is equal to $(1.2 \pm 0.3) \times 10^{-11} \exp[-(998 \pm 57)/T] \text{ cm}^3 \text{ molecule}^{-1} \text{ s}^{-1}$. The dotted line is the non-Arrhenius fit to all the data points and is equal to $9.2 \times 10^{-18} T^{2.17 \pm 0.50} \exp[-(478 \pm 165)/T] \text{ cm}^3 \text{ molecule}^{-1} \text{ s}^{-1}$. The dash-dotted line is the *ab initio* calculation by Harding *et al.*

addition complex. It is worth noting that Lander *et al.*⁷ did see a slight pressure dependence for reaction 2 at room temperature over the same helium number densities. There is no obvious explanation for why their pressure dependence result for reaction 2 contradicts our findings for the same reaction.

The reactions of the C₂H radical with C₂H₄ and C₂H₆ exhibit similar temperature and pressure dependencies as the CN radical does with C₂H₄ and C₂H₆.^{24,25} Reactions of the CN radical have been studied down to temperatures reaching 25 K using a pulsed laser photolysis, time-resolved laser-induced fluorescence technique by Sims and co-workers.²⁴ The reaction of CN + C₂H₄ is found to show a mild negative temperature dependence (see Figure 7). However, the rate coefficient shows a sharp decrease from 44 to 25 K. The Arrhenius plot for the reaction of CN + C₂H₄ in Figure 7 shows that the measured value of $k_{CN+C_2H_4}$ at 25 K is less than $k_{CN+C_2H_4}$ at 44 K. Sims *et al.* indicated that this could signal a small potential barrier along the path leading to CH₂CH₂CN formation. This reaction also exhibits no dependence on total pressure. Sims *et al.* rationalized their observations by stating that the reaction proceeds through an addition-elimination mechanism, resulting in an exothermic displacement of an H atom by the CN radical.

The rate coefficient $k_{CN+C_2H_6}$ for CN + C₂H₆ displays a pronounced curvature in its Arrhenius plot; see Figure 7. From

TABLE 1: Summary of Rate Coefficients of C₂H with H₂, C₂H₄ and C₂H₆ from 150 to 359 K

temp (K)	$k_{C_2H_4}$ (cm ³ molecule ⁻¹ s ⁻¹)	temp (K)	$k_{C_2H_6}$ (cm ³ molecule ⁻¹ s ⁻¹)	temp (K)	k_{H_2} (cm ³ molecule ⁻¹ s ⁻¹)
357	$(0.9 \pm 0.2) \times 10^{-10}$	357	$(3.2 \pm 0.5) \times 10^{-11}$	359	$(7.5 \pm 0.8) \times 10^{-13}$
357	$(1.2 \pm 0.2) \times 10^{-10}$	355	$(3.6 \pm 0.5) \times 10^{-11}$	355	$(6.7 \pm 0.9) \times 10^{-13}$
356	$(1.1 \pm 0.2) \times 10^{-10}$	355	$(3.5 \pm 0.5) \times 10^{-11}$	300	$(4.6 \pm 0.7) \times 10^{-13}$
298	$(1.4 \pm 0.2) \times 10^{-10}$	298	$(3.4 \pm 0.5) \times 10^{-11}$	228	$(2.1 \pm 0.4) \times 10^{-13}$
298	$(1.3 \pm 0.2) \times 10^{-10}$	298	$(3.9 \pm 0.6) \times 10^{-11}$	215	$(0.9 \pm 0.3) \times 10^{-13}$
298	$(1.1 \pm 0.2) \times 10^{-10}$	298	$(3.4 \pm 0.5) \times 10^{-11}$	213	$(1.1 \pm 0.2) \times 10^{-13}$
216	$(1.6 \pm 0.1) \times 10^{-10}$	298	$(3.5 \pm 0.6) \times 10^{-11}$	191	$(5.3 \pm 0.9) \times 10^{-14}$
197	$(1.8 \pm 0.2) \times 10^{-10}$	198	$(3.9 \pm 0.6) \times 10^{-11}$	178	$(5.0 \pm 1.1) \times 10^{-14}$
173	$(2.1 \pm 0.3) \times 10^{-10}$	180	$(3.3 \pm 0.4) \times 10^{-11}$		
150	$(1.4 \pm 1.0) \times 10^{-10}$	173	$(4.0 \pm 0.6) \times 10^{-11}$		
		163	$(3.4 \pm 0.8) \times 10^{-11}$		
		153	$(3.3 \pm 0.6) \times 10^{-11}$		

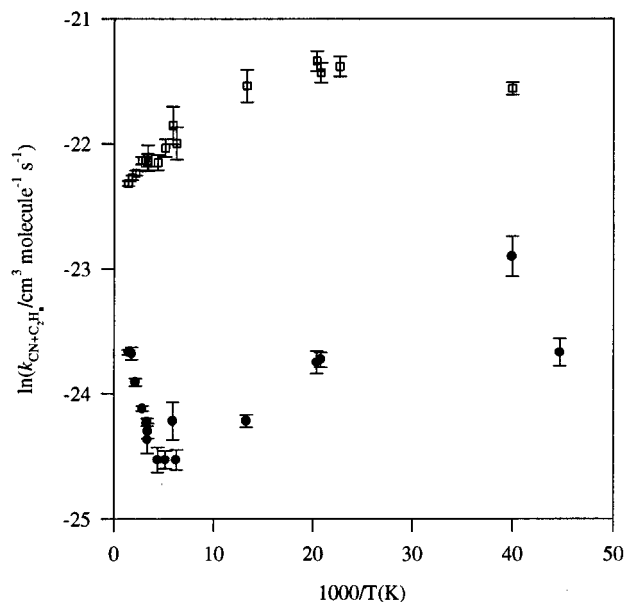


Figure 7. Arrhenius plot of CN with C₂H₄ and C₂H₆: ●, work of Herbert *et al.* and Sims *et al.* for CN + C₂H₄; □, work of Herbert *et al.* and Sims *et al.* for CN + C₂H₆.

300 to 1000 K, $k_{\text{CN}+\text{C}_2\text{H}_6}$ shows a positive temperature dependence and from 300 down to 25 K, $k_{\text{CN}+\text{C}_2\text{H}_6}$ exhibits a negative temperature dependence. However, from approximately 75 to 300 K, $k_{\text{CN}+\text{C}_2\text{H}_6}$ remains constant just as $k_{\text{C}_2\text{H}_6}$ does for the reaction of C₂H + C₂H₆; see Figure 7. Sims and co-workers have no suitable explanation for the sharp increase in $k_{\text{CN}+\text{C}_2\text{H}_6}$ below 75 K.²⁴ They have ruled out the formation of a stabilized CN–C₂H₆ van der Waals complex contributing to the increase in $k_{\text{CN}+\text{C}_2\text{H}_6}$ but state that weak, long-range attractive forces between CN and C₂H₆ assist in increasing $k_{\text{CN}+\text{C}_2\text{H}_6}$ at very low temperatures. Sims *et al.* theorize that a “transient van der Waals” complex could be formed when the energy of the colliding CN and C₂H₆ species is lower than the van der Waals potential well. This would allow the reactants to find a favorable orientation for a reaction to occur.

In addition to comparing reactions 1 and 2 to their CN counterparts, it is beneficial to relate them to other C₂H reactions. Table 2 lists several rate coefficients at room temperature of the C₂H reactions with hydrocarbons and H₂ and various thermodynamic properties. All of these reactions are very exothermic, but their rate coefficients vary by 3 orders of magnitude from C₂H + C₂H₂ to C₂H + H₂. Interestingly, of the five reactions listed in Table 2, the fastest are those with the largest C–H bond dissociation energies: C₂H with C₂H₂ and C₂H₄. Since the measured energy of activation is negative in these reactions, there is little or no barrier to form the addition complex. Therefore, the rate-determining step in each of these reactions, and C₂H + C₂H₆, is most likely the formation of the addition complex. The last two reactions listed in Table 2, C₂H with CH₄ and H₂, have a positive energy of activation, suggesting that the rate-determining step is the direct H atom abstraction by the ethynyl radical. Since the mechanism involves a direct abstraction rather than one of complex formation, it is inherent that the measured rate coefficients at room temperature are the slowest of the five and decrease sharply as the temperature decreases. The factor of 3–4 difference between $k_{\text{C}_2\text{H}_4}$ and $k_{\text{C}_2\text{H}_6}$ at room temperature can possibly be traced to the radical’s attraction to the electron-rich double bond in C₂H₄. Compared to ethene, ethane does not possess the π electrons for C₂H to attack. In order to form a complex with C₂H₆, the C₂H must attack either the C–H or C–C σ electrons. If the

C₂H radical were to attack the C–C bond in C₂H₆, the two methyl groups would provide some steric hindrance which could account for $k_{\text{C}_2\text{H}_4} > k_{\text{C}_2\text{H}_6}$ at room temperature. The same argument can be stated for $k_{\text{C}_2\text{H}_2}$ in the reaction of C₂H + C₂H₂. The π electrons in acetylene are exposed for the C₂H radical to capture, and the room temperature rate coefficient $k_{\text{C}_2\text{H}_2}$ is an order of magnitude faster than $k_{\text{C}_2\text{H}_6}$.

C₂H + H₂. A summary of all the current rate coefficients measured for C₂H + H₂ is given in Table 3. The data for C₂H + H₂ from 178 to 359 K can be fit to an Arrhenius plot of $k_{\text{H}_2} = (1.2 \pm 0.3) \times 10^{-11} \exp[(-998 \pm 57)/T] \text{ cm}^3 \text{ molecule}^{-1} \text{ s}^{-1}$ represented by the solid line in Figure 6. Upon closer examination of the combined data from Farhat *et al.*,¹¹ Koshi *et al.*,¹² and this work, a slight curvature is observed from 178 to 854 K. The combined data are best fit to a non-Arrhenius form of $k_{\text{H}_2} = 9.2 \times 10^{-18} T^{2.17 \pm 0.50} \exp[(-478 \pm 165)/T] \text{ cm}^3 \text{ molecule}^{-1} \text{ s}^{-1}$, represented by the dashed line in Figure 6. The question as to whether or not the curvature in Figure 6 is real or simply due to experimental error must be addressed.

Farhat *et al.*¹¹ did a similar set of experiments as described in this work over a temperature range 295–854 K. The ethynyl radical was produced by acetylene photolysis at 193 nm and detected in absorption with a color center laser. Their data can be fit to an Arrhenius expression of the form $k_{\text{H}_2} = 6.9 \times 10^{-11} \exp[-1480/T] \text{ cm}^3 \text{ molecule}^{-1} \text{ s}^{-1}$, but they chose to fit their data to a non-Arrhenius expression of the form $k_{\text{H}_2} = (9.44 \pm 0.24) \times 10^{-14} T^{0.9} \exp[(-1003 \pm 20)/T] \text{ cm}^3 \text{ molecule}^{-1} \text{ s}^{-1}$. The room temperature values of k_{H_2} for this work and Farhat *et al.* calculated from the fits shown in Table 3 agree within experimental error.

Koshi *et al.*,¹² using laser photolysis time-resolved mass spectrometry, measured k_{H_2} over the temperature range 298–438 K and found an Arrhenius dependence of $k_{\text{H}_2} = (1.8 \pm 1.0) \times 10^{-11} \exp[(-1090 \pm 299)/T] \text{ cm}^3 \text{ molecule}^{-1} \text{ s}^{-1}$. In their experiment, the concentration of C₄H₂ is monitored and first used to measure the rate coefficients of C₂H + C₂H₂. When H₂ is added to the gas flow, the concentration of C₄H₂ decreases due to reaction 1. The ratio of $k_{\text{C}_2\text{H}_2}/k_{\text{H}_2}$ is measured based on the C₄H₂ concentration and reported in their work. The room temperature value of k_{H_2} in the work by Koshi *et al.*, $(5.1 \pm 2.0) \times 10^{-13} \text{ cm}^3 \text{ molecule}^{-1} \text{ s}^{-1}$, agrees within error with the averaged measured value from this work and Farhat *et al.*, which are $(4.6 \pm 0.8) \times 10^{-13}$ and $(4.7 \pm 0.5) \times 10^{-13} \text{ cm}^3 \text{ molecule}^{-1} \text{ s}^{-1}$, respectively. Due to the differences in the methods, the curvature in Figure 6 should be regarded with some caution; nevertheless, in the discussion that follows we consider some possible sources of the curvature.

The latest high temperature work was done by Peeters *et al.*¹⁹ using laser photodissociation/chemiluminescence. Ethynyl radicals were generated from C₂H₂ or C₂HCF₃ photodissociation by 193 nm light from an excimer. The pseudo-first-order decay of C₂H was monitored by depletion of the chemiluminescence of CH(A²Δ) produced by the radical reaction with O₂. They measured k_{H_2} from 295 to 440 K and fit their data to the expression $k_{\text{H}_2} = 1.31 \times 10^{-18} T^{2.39} \exp(-174/T) \text{ cm}^3 \text{ molecule}^{-1} \text{ s}^{-1}$. In conjunction with measurements taken by Koshi *et al.* and Farhat *et al.*, the measurements made by Peeters *et al.* for reaction 3 follow the trend of k_{H_2} increasing with temperature; see Figure 6.

When analyzing reaction 3, it is again useful to consult a similar reaction such as



Although CN is a diatomic radical, it is isoelectronic with C₂H, and the measured rate coefficients with C₂H₂, C₂H₄, C₂H₆, O₂,

TABLE 2: Comparison of Various C₂H Reactions

reaction	ΔH^a	E_a^b	$D_0^{c,d}$	k^e
C ₂ H + C ₂ H ₂ → C ₄ H ₂ + H	-102	-0.7 ± 0.1	HC ₂ -H 549.3	(1.3 ± 0.2) × 10 ⁻¹⁰
C ₂ H + C ₂ H ₄ → products	<i>f</i>	-1.1 ± 0.4	H ₂ C ₂ -H 465.2	(1.3 ± 0.2) × 10 ⁻¹⁰
C ₂ H + C ₂ H ₆ → C ₂ H ₅ + C ₂ H ₂	-133	-0.02 ± 0.10	H ₃ C ₂ -H 410	(3.6 ± 0.6) × 10 ⁻¹¹
C ₂ H + CH ₄ → CH ₃ + C ₂ H ₂	-117	4.3 ± 0.1	H ₃ C-H 438	(2.3 ± 0.1) × 10 ⁻¹²
C ₂ H + H ₂ → C ₂ H ₂ + H	-116	8.3 ± 0.5	H-H 436	(4.6 ± 0.7) × 10 ⁻¹³

^a Units of kJ mol⁻¹, ref 31. ^b Units of kJ mol⁻¹. ^c Units of kJ mol⁻¹, ref 32. ^d Reference 33. ^e Rate coefficients measured at 300 K and in units of cm³ molecule⁻¹ s⁻¹. ^f References 3–5, C₂H + C₂H₄ → C₂H₂ + C₂H₃, $\Delta H = -90.4$ kJ mol⁻¹; C₂H + C₂H₄ → C₄H₄ + H, $\Delta H = -95.4$ kJ mol⁻¹ for the vinyl acetylene isomer.

TABLE 3: Summary of Rate Coefficients for C₂H + H₂

reference	k_{H_2} (cm ³ molecule ⁻¹ s ⁻¹)	temp (K)
this work	(1.2 ± 0.3) × 10 ⁻¹¹	178–359
Farhat <i>et al.</i> ¹¹	exp[(-998 ± 57)/T] (9.44 ± 0.24) × 10 ⁻¹⁴ T ^{0.9}	295–854
Koshi <i>et al.</i> ¹²	exp[(-1003 ± 20)/T] (1.8 ± 1.0) × 10 ⁻¹¹	298–438
Lange and Wagner ¹³	exp[(-1090 ± 299)/T] 1.7 × 10 ⁻¹³	320
Laufer and Bass ¹⁴	1.5 × 10 ⁻¹³	298
Renlund <i>et al.</i> ¹⁵	(1.2 ± 0.3) × 10 ⁻¹¹	300
Okabe ¹⁶	9.7 × 10 ⁻¹³ ^a	298
Stephens <i>et al.</i> ¹⁷	(4.8 ± 0.3) × 10 ⁻¹³	298
Peeters <i>et al.</i> ¹⁹	1.31 × 10 ⁻¹⁸ T ^{2.39} exp(-174/T)	295–440

^a Recalculated using the measured ratio and the present-day C₂H + C₂H₂ rate constant of (1.3 ± 0.2) × 10⁻¹⁰ cm³ molecule⁻¹ s⁻¹.

TABLE 4: Reactions Involving H Atom Abstractions^a

reaction	V^\ddagger (kJ mol ⁻¹) ^b	ΔE (kJ mol ⁻¹) ^c	ν^\ddagger (cm ⁻¹) ^d
O(³ P) + H ₂	52.3	12.1	736, 736
CH ₄ + H	56.4	10.8	592, 592
CH ₃ + H ₂	44.7	-10.8	592, 592
H + H ₂ CO	20.5	59.4	325, 590
OH + H ₂	25.9	-67.3	440, 686
CN + H ₂	17.1	-105.8	165, 165
C ₂ H + H ₂	9.6	-129.7	139, 139

^a Table 4 is taken from ref 27. ^b V^\ddagger Classical barrier at the saddle point. ^c ΔE The difference in internal energy between products and reactants. ^d ν^\ddagger The two lowest bending frequencies at the saddle point. V^\ddagger and ΔE , taken from Wagner and Bair, do not include zero-point corrections.

and CH₄ show similar temperature dependencies as their C₂H counterparts.²⁴ Reaction 16 has been studied by several groups over the combined temperature range 209–1000 K.^{26–29} The measured rate coefficients of reaction 16 exhibit a positive temperature dependence in addition to a mild curvature in the Arrhenius plot. One study, by Sims and Smith, gives the modified Arrhenius fit to reaction 16 CN($\nu=0$) as (2.4 ± 0.7) × 10⁻¹² (T/298)^{1.6±0.2} exp[(-1340 ± 90)/T] cm³ molecule⁻¹ s⁻¹ from 295 to 768 K.²⁶ A theoretical study by Wagner and Bair²⁷ has shown that the H₂CN[‡] transition state closely resembles the separated reactants, which is consistent with Hammond's postulate for exothermic reactions.³⁰ The H–H bond distance is increased only by 0.07 Å at the saddle point, and the C–N bond distance remains constant. Both Sims and Smith and Wagner and Bair have concluded that the curvature in the Arrhenius plot for reaction 16 is due to the temperature dependence of the partition function associated with the doubly degenerate low-frequency bending mode in the H₂CN[‡] transition state.

Wagner and Bair also compare their results for CN + H₂ to those of other H atom abstraction reactions; see Table 4. The first three reactions in Table 4 are close to thermoneutral and have barriers exceeding 40 kJ mol⁻¹ and possess bending degrees of freedom with vibrations greater than 500 cm⁻¹. The rate coefficients for these reactions exhibit a steep positive temperature dependence, but vary little from Arrhenius form.

The middle two reactions display noticeable curvature in their Arrhenius plots and have at least one bending frequency below 500 cm⁻¹. The final two reactions, C₂H + H₂ and CN + H₂, have the lowest barriers, V^\ddagger , and the lowest bending frequencies in the group. Their rate coefficients show substantial curvature in their respective Arrhenius plots.

Both Harding *et al.*⁸ and Herbst⁹ have performed theoretical calculations on the reaction C₂H + H₂, Harding from 300 to >2000 K and Herbst from 10 to 300 K; see Figures 6 and 8. Harding and co-workers calculate that reaction 3 has an early saddle point with the H_a–H_b bond distance in the H_a–H_b–C_c–C_d–H_e[‡] transition state only 6% larger than in the H₂ reactant and the H_b–C_c bond 52% greater than in the C₂H₂ product. This calculation also confirms Hammond's postulate that more exothermic reactions have reactant-like transition states. The fit by Harding *et al.*, including Wigner tunneling corrections, is for a barrier height of 9.6 kJ mol⁻¹ and shows significant curvature. Harding and co-workers performed this calculation at different barrier heights, V^\ddagger . When the barrier is decreased, their calculated rate coefficients increase with respect to the Arrhenius plot in Figure 6, and the fit shows more curvature. Conversely, when the barrier is increased, the rate coefficients decrease with respect to their Arrhenius plot in Figure 6, and the fit shows less curvature. Although the calculated rate coefficients are lower than the values measured here and those by Farhat *et al.*⁶ and Koshi *et al.*,⁷ the general trend of k_{H_2} and curvature is followed.

Herbst, using statistical phase space theory and the vibrational frequencies and rotational constants from Harding *et al.*,⁸ calculated rate coefficients from 300 to 10 K for reaction 3. At room temperature, Herbst reports that the tunneling contribution to k_{H_2} is ~40%, and then k_{H_2} starts to decrease as the temperature is lowered. The rate coefficients for k_{H_2} decrease to a minimum value at ~40 K of approximately 1.2 × 10⁻¹⁵ cm³ molecule⁻¹ s⁻¹. Afterward, k_{H_2} increases to a value of 2.2 × 10⁻¹⁵ cm³ molecule⁻¹ s⁻¹ at 10 K; see Figure 8. For clarity, only four of his calculated points are shown in Figure 6 due to the range of "1/T space" the calculation spans. Herbst claims that the increase in k_{H_2} is due to a decrease in the density of reactant states which control the redissociation rate instead of an increase in the tunneling rate. However, Herbst is quick to note that his model is highly sensitive to several undefined parameters such as the transition state barrier, V^\ddagger , and the imaginary frequency of vibration, ν_i^\ddagger . A "slight" decrease in the transition state barrier increases k_{H_2} by an order of magnitude at 10 K. A change in the transition state frequency by ±200 cm⁻¹ results in k_{H_2} fluctuating in both directions by an order of magnitude.

In light of the stated results in the previous paragraphs, one can make some clarifications on the curvature in the combined experimental data of Farhat *et al.*, Koshi *et al.*, and this work. Despite the larger scatter of points in this data below room temperature, the curvature of the modified Arrhenius fit to k_{H_2} from 178 to 854 K appears to be real. Arguments as to what is causing it can be traced partly to the CN + H₂ studies by Sims *et al.* and Wagner *et al.* Both groups made it clear that

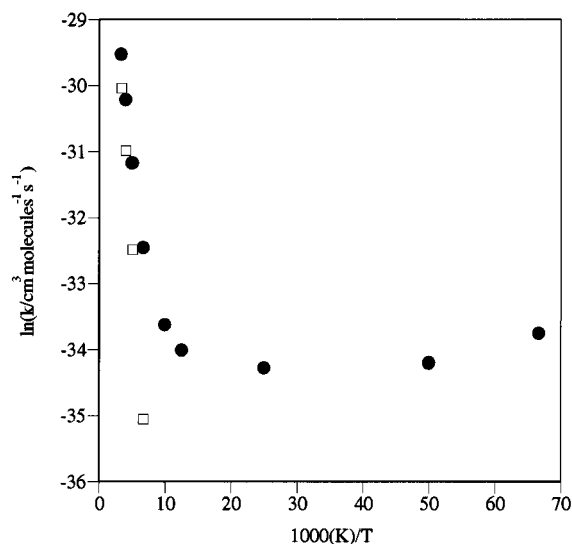


Figure 8. Arrhenius plot of $C_2H + H_2$ using calculated rate coefficients by Herbst: ●, calculation with tunneling corrections; □, calculation without tunneling corrections.

the curvature in the Arrhenius plot of $CN + H_2$ is due to the temperature dependence of the partition function associated with the doubly degenerate low-frequency bending mode in the H_2CN^\ddagger transition state. Pronounced curvature in Arrhenius plots is displayed by H atom abstraction reactions in Table 4 that are highly exothermic, have low barriers, and have low bending frequencies in the transition state. The reaction of $C_2H + H_2$ most likely follows this trend. Therefore, at least part of the curvature in the experimental data from 178 to 854 K can be attributed to the temperature dependence of the partition function linked to the low-frequency bending mode in the $H_2C_2H^\ddagger$ transition state.

However, one must consider how much tunneling plays a role in this reaction, especially since the fit by Harding and co-workers, although low compared to the data, displays the same curvature that the experimental data exhibits. The *ab initio* calculation by Harding *et al.* includes Wigner tunneling corrections and is conceivably offset from the experimental data because the barrier height used in the calculation is too high. If the barrier height was lowered below 9.6 kJ mol^{-1} , then the fit by Harding *et al.* would overlap the combined experimental results from 178 to 854 K by Farhat *et al.*, Koshi *et al.*, and this work. Taking this into account, H atom tunneling could also contribute to the curvature in the Arrhenius plot of $C_2H + H_2$.

One cannot conclusively state whether the curvature in the Arrhenius plot of $C_2H + H_2$ is due solely to either tunneling or to the partition function associated the low-frequency bending modes in the $H_2C_2H^\ddagger$ transition state. Advanced theories will need to take into account both explanations.

Conclusion

The rate coefficients of C_2H with C_2H_4 , C_2H_6 , and H_2 have been measured from 150 to 359 K. The reaction of $C_2H + C_2H_4$ displays a mild negative temperature dependence similar to that of $CN + C_2H_4$ which is characteristic of an addition–elimination mechanism. The C_2H data are fit to an Arrhenius expression equal to $(7.8 \pm 0.6) \times 10^{-11} \exp[(134 \pm 44)/T] \text{ cm}^3 \text{ molecule}^{-1} \text{ s}^{-1}$. Likewise, the reaction mechanism of $C_2H + C_2H_6$ also consists of an addition–elimination step. Within the calculated error bars, the rate coefficients of reaction 3 display

no temperature dependence from 153 to 357 K. The Arrhenius fit for this reaction is equal to $(3.5 \pm 0.3) \times 10^{-11} \exp[(2.9 \pm 16)/T] \text{ cm}^3 \text{ molecule}^{-1} \text{ s}^{-1}$.

The Arrhenius fit to the data for C_2H and H_2 can be expressed as $k_{H_2} = (1.2 \pm 0.3) \times 10^{-11} \exp[-998 \pm 57]/T] \text{ cm}^3 \text{ molecule}^{-1} \text{ s}^{-1}$. The positive temperature dependence is consistent with reactions involving a hydrogen abstraction as the rate-determining step and a positive energy of activation ($E_a = 8.3 \pm 0.5 \text{ kJ mol}^{-1}$ for $C_2H + H_2$). The curvature in the Arrhenius plot of $C_2H + H_2$ can be attributed to a combination of H atom tunneling and a temperature dependence in the partition function associated with the low-frequency bending mode in the $H_2C_2H^\ddagger$ transition state.

Acknowledgment. We gratefully acknowledge the National Aeronautics and Space Administration for support of this research and the Department of Energy for additional support.

References and Notes

- (1) Homann, K. H.; Wagner, H. G. *Proc. R. Soc. London, A* **1968**, *307*, 141.
- (2) Yung, Y. L.; Allen, M.; Pinto, J. P. *Astrophys. J., Suppl. Ser.* **1984**, *55*, 465.
- (3) Gladstone, G. R.; Allen, M.; Yung, Y. L. *Icarus* **1996**, *119*, 1.
- (4) *Mechanism and Theory in Organic Chemistry*; Lowry, T. H., Richardson, K. S., Eds.; Harper and Row: New York, 1987.
- (5) Ervin, K. M.; Gronert, S.; Barlow, S. E.; Gilles, M. K.; Harrison, A. G.; Bierbaum, V. M.; DePuy, C. H.; Lineberger, W. C.; Ellison, G. B. *J. Am. Chem. Soc.* **1990**, *112*, 5750.
- (6) Allen, M.; Yung, Y. K.; Gladstone, G. R. *Icarus* **1992**, *100*, 527.
- (7) Lander, D. R.; Unfried, K. G.; Glass, G. P.; Curl, R. F. *J. Phys. Chem.* **1990**, *94*, 7759.
- (8) Harding, L. B.; Schatz, G. C.; Chiles, R. A. *J. Chem. Phys.* **1982**, *76*, 5172.
- (9) Herbst, E. *Chem. Phys. Lett.* **1994**, *222*, 297.
- (10) Opansky, B. J.; Leone, S. R. *J. Phys. Chem.* **1996**, *100*, 4448.
- (11) Farhat, S. K.; Morter, C. L.; Glass, G. P. *J. Chem. Phys.* **1993**, *97*, 12789.
- (12) Koshi, M.; Fukada, K.; Kamiya, K.; Matsui, H. *J. Phys. Chem.* **1992**, *96*, 9839.
- (13) Lange, W.; Wagner, H. G. *Ber. Bunsen-Ges. Phys. Chem.* **1975**, *79*, 165.
- (14) Laufer, A. H.; Bass, A. M. *J. Phys. Chem.* **1981**, *85*, 3828.
- (15) Renlund, A. M.; Shokoohi, F.; Reisler, H.; Wittig, C. *J. Phys. Chem.* **1982**, *86*, 4165.
- (16) Okabe, H. *J. Phys. Chem.* **1982**, *78*, 1312.
- (17) Stephens, J. W.; Hall, J. L.; Solka, H.; Yan, Y. B.; Curl, R. F.; Glass, G. P. *J. Phys. Chem.* **1987**, *91*, 5740.
- (18) Peeters, J.; Van Look, H.; Ceursters, B. *J. Phys. Chem.* **1996**, *100*, 15124.
- (19) Laufer, A. H. *J. Phys. Chem.* **1981**, *85*, 3828.
- (20) Opansky, B. J.; Seakins, P. W.; Pedersen, J. O. P.; Leone, S. R. *J. Phys. Chem.* **1993**, *97*, 8583.
- (21) Pedersen, J. O. P.; Opansky, B. J.; Leone, S. R. *J. Phys. Chem.* **1993**, *97*, 6822.
- (22) Satyapal, S.; Bersohn, R. *J. Phys. Chem.* **1991**, *95*, 8004.
- (23) Shin, K. S.; Michael, J. V. *J. Phys. Chem.* **1991**, *95*, 5864.
- (24) Sims, I. R.; Queffelec, J. L.; Travers, D.; Rowe, B. R.; Herbert, L. B.; Karthaus, J.; Smith, I. W. M. *Chem. Phys. Lett.* **1993**, *461*, 211.
- (25) Herbert, L.; Smith, I. W. M.; Spencer-Smith, R. D. *Int. J. Chem. Kinet.* **1992**, *24*, 791.
- (26) Sims, I. R.; Smith, I. W. M. *Chem. Phys. Lett.* **1988**, *149*, 565.
- (27) Wagner, A. F.; Bair, R. A. *Int. J. Chem. Kinet.* **1986**, *18*, 473.
- (28) Atakan, b.; Jacobs, A.; Wahl, M.; Weller, R.; Wolfrum, J. *Chem. Phys. Lett.* **1989**, *154*, 449.
- (29) Sun, Q.; Yang, D. L.; Wang, N. S.; Bowman, J. M.; Lin, M. C. *J. Chem. Phys.* **1990**, *93*, 4730.
- (30) Hammond, G. S. *J. Am. Chem. Soc.* **1955**, *77*, 334.
- (31) ΔH taken from JANAF: *J. Chem. Ref. Data* **1992**, *21* (Suppl. No. 3).
- (32) *Organic Chemistry*, 4th ed.; Morrison, R. T., Boyd, R. N., Eds.; Allyn and Bacon: Boston, MA, 1983.
- (33) *Physical Chemistry*, 3rd ed.; Atkins, P. W., Ed.; Oxford University Press: London, 1986.